

# BEVTrack: A Simple and Strong Baseline for 3D Single Object Tracking in Bird’s-Eye View

Yuxiang Yang, Yingqi Deng, Jing Zhang, Jiahao Nie, Zheng-Jun Zha

**Abstract**—3D Single Object Tracking (SOT) is a fundamental task of computer vision, proving essential for applications like autonomous driving. It remains challenging to localize the target from surroundings due to appearance variations, distractors, and the high sparsity of point clouds. To address these issues, prior Siamese and motion-centric trackers both require elaborate designs and solving multiple subtasks. In this paper, we propose BEVTrack, a simple yet effective baseline method. By estimating the target motion in Bird’s-Eye View (BEV) to perform tracking, BEVTrack demonstrates surprising simplicity from various aspects, *i.e.*, network designs, training objectives, and tracking pipeline, while achieving superior performance. Besides, to achieve accurate regression for targets with diverse attributes (*e.g.*, sizes and motion patterns), BEVTrack constructs the likelihood function with the learned underlying distributions adapted to different targets, rather than making a fixed Laplacian or Gaussian assumption as in previous works. This provides valuable priors for tracking and thus further boosts performance. While only using a single regression loss with a plain convolutional architecture, BEVTrack achieves state-of-the-art performance on three large-scale datasets, KITTI, NuScenes, and Waymo Open Dataset while maintaining a high inference speed of about 200 FPS. The code will be released at [BEVTrack](#).

**Index Terms**—3D Object Tracking, Point Cloud, Bird’s-Eye View, Convolutional Neural Networks, Regression

## I. INTRODUCTION

3D single object tracking (SOT) is crucial for various applications, such as autonomous driving [1]–[3]. It aims to localize a specific target across a sequence of point clouds, given only its initial status. Existing tracking approaches [4], [5] commonly adopt the point-wise representation, directly taking raw point clouds as input. For example, P2B [4] and its follow-up works [6]–[8] adopt a point-based network [9], [10] with the Siamese architecture for feature extraction, followed by a point-wise appearance matching module [4], [8], [11] for propagation of target cues, and a 3D Region Proposal Network [12], [13] for target localization, as illustrated in Fig. 1(a). M2-Track [5] proposes a motion-centric paradigm, that first segments the target points from their surroundings with a PointNet [14] segmentation network and then localizes the target through a motion modeling approach followed by a box refinement module, as illustrated in Fig. 1(b).

The project was supported by the National Natural Science Foundation of China (62376080), the Zhejiang Provincial Natural Science Foundation Key Fund of China (LZ23F030003), and the Fundamental Research Funds for the Provincial Universities of Zhejiang (GK239909299001-003). Corresponding author: Jing Zhang (jing.zhang1@sydney.edu.au)

Y. Yang, Y. Deng and J. Nie are with the School of Electronics and Information, Hangzhou Dianzi University, Hangzhou 310018, China. J. Zhang is with the School of Computer Science, The University of Sydney, NSW 2006, Australia. Z. Zha is with the Department of Automation, University of Science and Technology of China 230022, China.

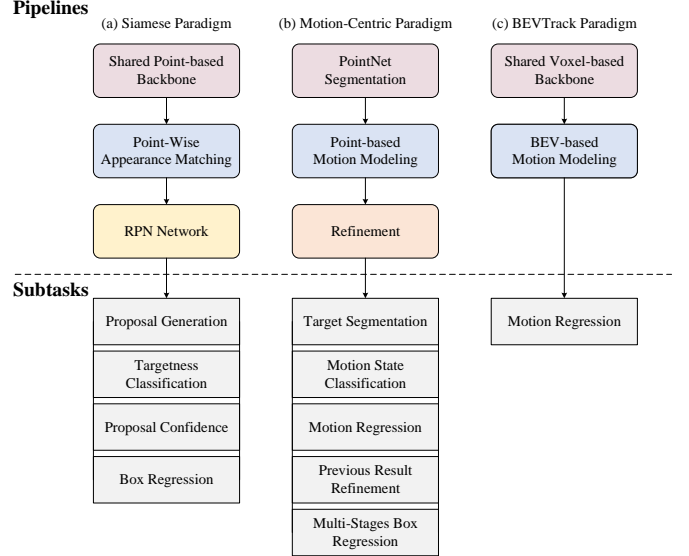


Fig. 1: Comparison with typical 3D SOT paradigms. Previous methods mainly rely on the point-wise representation, and decompose the tracking problem into multiple subtasks, leading to a complicated tracking framework. On the contrary, our proposed BEVTrack performs tracking in BEV, greatly retaining the spatial information and thus simplifying the tracking pipeline while improving the performance.

Although these approaches have exhibited superior performance in tracking benchmarks, two deficiencies still exist. First, they usually require elaborate designs [8], [11], [15], [16], leading to a complicated tracking framework. Second, they usually require solving multiple subtasks in the training phase, which makes the training cumbersome due to heavy hyperparameter tuning.

In this paper, we present BEVTrack, a simple yet strong baseline for 3D SOT, as shown in Fig. 1(c). By estimating the target motion in Bird’s-Eye View (BEV) to perform tracking, BEVTrack demonstrates surprising simplicity from various aspects, *i.e.*, network designs, training objectives, and tracking pipeline, while achieving superior performance. It is based upon the intuition that BEV could better capture motion features, since objects primarily move horizontally in autonomous driving scenarios. Specifically, we first adopt a voxel-based network [17] with the Siamese architecture for feature extraction. Subsequently, we compress height information into the channel dimension to obtain the BEV features. Given that corresponding objects are spatially adjacent in

the BEV features across consecutive frames, we can easily fuse them together with an element-wise operation such as concatenation [18], [19]. Then we adopt several convolutional and downsampling layers to capture the object motion with a wide range of patterns. Finally, we discard the complicated region proposal network while using a global max pooling followed by a lightweight multilayer perceptron (MLP) to localize the target, resulting in a simple one-stage tracking pipeline with a single regression loss.

To optimize the regression-based trackers, current approaches typically employ conventional  $L_1$  or  $L_2$  loss. This kind of supervision actually makes a fixed Laplacian or Gaussian assumption on the data distribution, which is inflexible when handling targets possessing diverse attributes (*e.g.*, sizes, moving patterns, and sparsity degrees). For example, when tracking targets with high sparsity degrees, where the predictions may be uncertain while the annotations are not very reliable, the outputs should conform to a distribution with a large variance. To this end, we introduce a novel distribution-aware regression strategy for tracking, which constructs the likelihood function with the learned underlying distributions adapted to distinct targets, instead of making a fixed assumption. Note that this strategy does not participate in the inference phase, thus boosting the tracking performance without additional computation overhead. Despite no elaborate design, BEVTrack exhibits a substantial performance advantage over the current state-of-the-art (SOTA) methods on challenging tracking datasets, *i.e.*, KITTI [20], NuScenes [21], and Waymo Open Dataset [22], while running at real-time (about 200 FPS).

The main contributions of this paper are three-fold:

- We propose BEVTrack, a simple yet strong baseline for 3D SOT. BEVTrack marks the first to perform tracking through motion modeling in BEV, resulting in a simplified tracking pipeline design.
- We present a novel distribution-aware regression strategy for tracking, which constructs the likelihood function with the learned underlying distributions adapted to targets possessing diverse attributes. This strategy provides accurate guidance for tracking, resulting in improved performance while avoiding extra computation overhead.
- BEVTrack achieves SOTA performance on three popular benchmarks while maintaining a high inference speed.

## II. RELATED WORK

### A. 3D Single Object Tracking

Early 3D SOT approaches [23], [24] predominantly utilize RGB-D data and often adapt 2D Siamese networks [25]–[28] by integrating depth maps. However, variations in illumination and appearance can adversely affect the performance of such RGB-D techniques. SC3D [29] is the first 3D Siamese tracker based on shape completion that generates a large number of candidates in the search area and compares them with the cropped template, taking the most similar candidate as the tracking result. The pipeline relies on heuristic sampling and does not learn end-to-end, which is very time-consuming.

To address these issues, P2B [4] develops an end-to-end framework by employing a shared point-based backbone

for feature extraction, followed by a point-wise appearance-matching technique for target cues propagation. Ultimately, a Region Proposal Network is used to derive 3D proposals, of which the one with the peak score is selected as the final output. P2B reaches a balance between performance and efficiency, and many works [6], [8], [15], [30], [31] follow the same paradigm. Drawing inspiration from the success of transformers [32], many studies have incorporated elaborate attention mechanisms to enhance feature extraction and target-specific propagation. For instance, PTT [30] introduces the Point Track Transformer to enhance point features. PTTR [8] presents the Point Relation Transformer for target-specific propagation and a Prediction Refinement Module for precision localization. Similarly, ST-Net [15] puts forth an iterative correlation network, and CXTrack [11] presents the Target Centric Transformer to harness contextual information from consecutive frames. SyncTrack [33] introduces a single-branch and single-stage framework, without Siamese-like forward propagation and a standalone matching network. MBPTrack [34] exploits both spatial and temporal contextual information using a memory mechanism. Unlike the Siamese paradigm, M2-Track [5] proposes a motion-centric paradigm, explicitly modeling the target’s motion between two successive frames. This motion-centric paradigm shows robustness to the problems caused by the appearance variation and the sparsity of point clouds. Moreover, M2-Track introduces a proof-of-concept tracker named M-Vanilla [35], which follows the one-stage motion-based tracking with a simple regression head. However, M-Vanilla shows performance degradation compared to M2-Track. Different from M-Vanilla, our BEVTrack regresses the target motion in BEV, achieving high performance with single-stage motion-based tracking for the first time.

Some prior research also utilizes BEV representations for tracking. Zarzar *et al.* [36] leverage the dense and structured BEV representation of LIDAR point clouds to efficiently search for objects of interest. LTTR [37] locates targets through similarity matching of BEV features. V2B [38] recommends converting the enhanced point features into dense BEV feature maps to generate high-quality target proposals. Recently, STTracker [39] fuses multi-frame BEV features to enhance the temporal features. These methods are based on appearance matching, with an RPN network [12], [40] for localization. In contrast, our BEVTrack is matching-free, and directly regresses the relative target motion in BEV for the first time.

### B. 3D object detection

3D object detection methods are usually similar to their 2D counterparts, such as R-CNN series [41]–[45] and CenterPoint series [40], [46], [47]. VoxelNet [17] utilizes PointNet [14] for voxel feature encoding, and then converts 3D sparse features into 2D dense BEV features [48]. Finally, it adopts a region proposal network for prediction. SECOND [19] improves VoxelNet by proposing efficient sparse convolutions. Motivated by 2D CenterNet [46], CenterPoint [40] focuses on 3D detection and tracking. It also transforms the sparse output from a backbone network into a dense feature map, enabling the

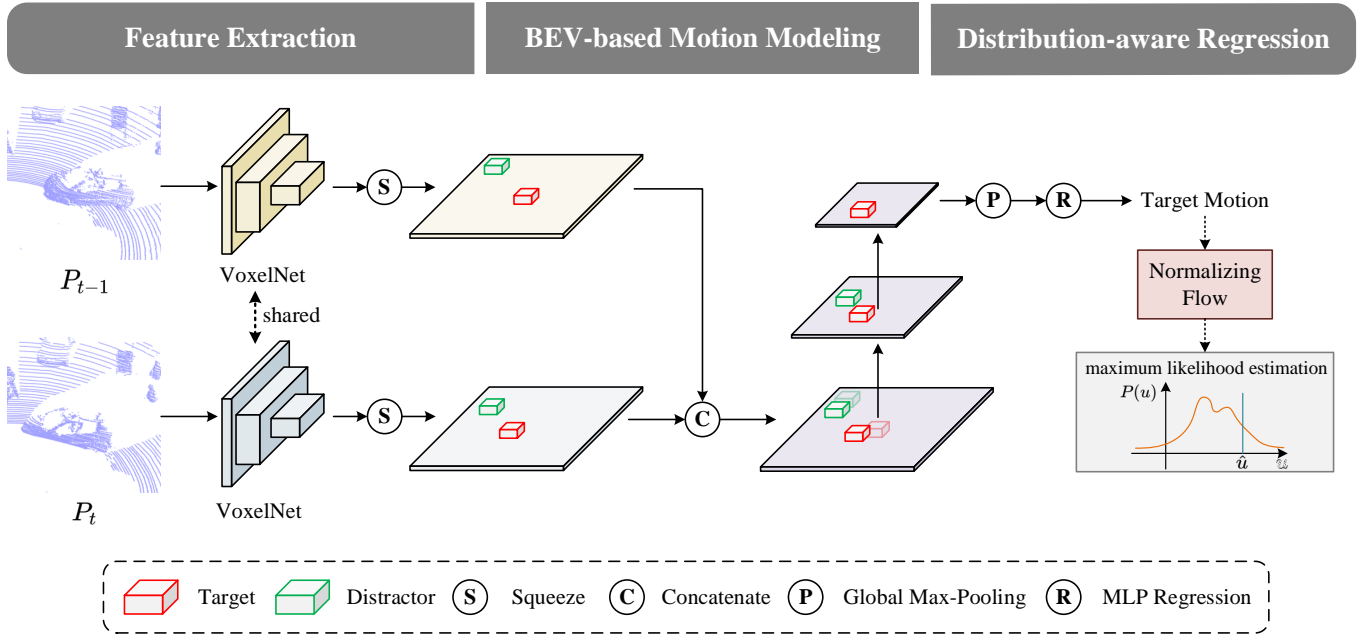


Fig. 2: Architecture of BEVTrack. The proposed framework contains three parts including voxel-based feature extraction, BEV-based motion modeling, and distribution-aware regression. Our BEVTrack is a simple tracking baseline framework with a plain convolutional architecture and a single regression loss, yet demonstrating state-of-the-art performance.

prediction of dense heatmaps indicating the center locations of objects. Recently, VoxelNext [49] predicts objects directly based on sparse voxel features, realizing fully sparse 3D object detection. In this paper, we adopt a variant of VoxelNet [17] as the backbone, which modifies the original architecture by removing residual connections, utilizing sparse 3D convolutions, and choosing suitable network hyper-parameters, such as voxel size.

### C. 3D Multi-Object Tracking

3D multi-object tracking models tracklets of multiple objects along multi-frame LiDAR. The majority of prior works in 3D MOT leverage the LiDAR modality. Due to the recent advances in LiDAR-based 3D detection [45], [49], [50], especially the reliable range information, most state-of-the-art 3D MOT algorithms [51], [52] adopt a “tracking-by-detection” paradigm. After detecting objects in each frame, these methods perform heuristic association of detected bounding boxes based on object motion or appearance [53]–[57]. CenterPoint [40] predicts the velocities to associate object centers through multiple frames, following CenterTrack [53]. SimTrack [58] combines object detection and motion association in a unified pipeline for joint detection and tracking. Compared to the 3D MOT methods, our BEVTrack focuses on tracking a specific target of interest.

## III. METHOD

### A. Overview

Given the 3D bounding box (BBox) of a specific target at the initial frame, 3D SOT aims to localize the target by predicting its 3D BBoxes in the subsequent frames. A 3D

BBox  $\mathcal{B}_t \in \mathbb{R}^7$  is parameterized by its center (*i.e.*,  $x, y, z$  coordinates), orientation (*i.e.*, heading angle  $\theta$  around the  $up$ -axis), and size (*i.e.*, width, length, and height). Suppose the point clouds in two consecutive frames are denoted as  $\mathcal{P}_{t-1} \in \mathbb{R}^{N_{t-1} \times 3}$  and  $\mathcal{P}_t \in \mathbb{R}^{N_t \times 3}$ , respectively, where  $N_{t-1}$  and  $N_t$  are the numbers of points in the point clouds. Notably, the two point clouds have been transformed to the canonical system w.r.t the target BBox  $\mathcal{B}_{t-1}$  (either given as the initial state or predicted by the tracker). At timestamp  $t$ , we do not crop the  $\mathcal{P}_{t-1}$  with the object bounding box, while directly take the  $\mathcal{P}_{t-1}$  and  $\mathcal{P}_t$  as input. Since the size of the tracking target rarely changes, we follow the common practice [4] and assume a constant target size. Consequently, the inter-frame target translation offsets (*i.e.*,  $\Delta x, \Delta y, \Delta z$ ) and the yaw angle offset  $\Delta\theta$  are regressed. By applying the translation and rotation to the 3D BBox  $\mathcal{B}_{t-1}$ , we can compute the 3D BBox  $\mathcal{B}_t$  to localize the target in the current frame. The tracking process can be formulated as:

$$\mathcal{F}(\mathcal{P}_{t-1}, \mathcal{P}_t) \mapsto (\Delta x, \Delta y, \Delta z, \Delta\theta), \quad (1)$$

where  $\mathcal{F}$  is the mapping function learned by the tracker.

Following Eq. (1), we propose BEVTrack, a simple yet strong baseline for 3D SOT. The overall architecture of BEVTrack is presented in Fig. 2. It first employs a shared voxel-based backbone [17] to extract 3D features, which are then squeezed to derive the BEV features (Sec. III-B). Subsequently, BEVTrack fuses the BEV features via a concatenation operation and several convolutional layers (Sec. III-C). Finally, it adopts a simple prediction head which contains a global max pooling layer followed by a lightweight MLP. For accurate regression, we optimize the model with a novel distribution-aware regression strategy in the training phase (Sec. III-D).

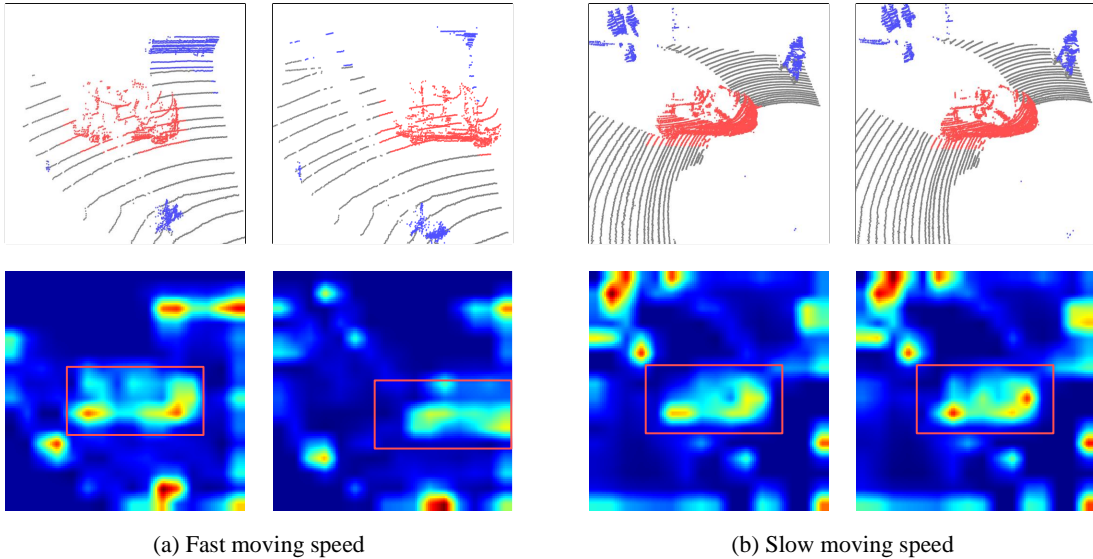


Fig. 3: The motion pattern of objects is variable in different scenes. The top rows show point cloud scenes across two consecutive frames, where the red points indicate the target. The bottom rows visualize the heatmaps of the BEV response map with ground-truth bounding box (in red rectangles).

### B. Feature Extraction

To localize the target from surroundings accurately, we need to learn discriminative features from the point clouds. Instead of using a point-based backbone [9], [10], [14] as in [4], [5], [11], we adopt a variant of VoxelNet [17] as the shared backbone, which modifies the original architecture by removing residual connections, utilizing sparse 3D convolutions [59], [60], and choosing suitable network hyper-parameters, such as voxel size. Specifically, we voxelize the 3D space into regular voxels and extract the voxel-wise features of each non-empty voxel by a stack of sparse convolutions, where the initial feature of each voxel is simply calculated as the mean values of point coordinates within each voxel in the canonical coordinate system. The spatial resolution is downsampled 8 times by three sparse convolutions of stride 2, each of which is followed by several submanifold sparse convolutions [59]. Afterwards, we squeeze the sparse 3D features along the height dimension to derive the BEV features  $\mathcal{X}_{t-1} \in \mathbb{R}^{H \times W \times C}$  and  $\mathcal{X}_t \in \mathbb{R}^{H \times W \times C}$ , where  $H$  and  $W$  denote the 2D grid dimension and  $C$  is the number of feature channels.

### C. BEV-based Motion Modeling

BEV-based Motion Modeling (BMM) aims to model the motion relations of the target as well as distractors in BEV, while propagating the target cues from the previous frame to the current frame. Given the BEV features  $\mathcal{B}_{t-1}$  and  $\mathcal{B}_t$ , the corresponding objects are spatially adjacent across them. Therefore, we can easily fuse them together with an element-wise operator such as concatenation to preserve their spatial proximity. Furthermore, we apply several convolutional blocks to encode their motion relations. It is noteworthy that the receptive field of the convolution is limited due to the small kernel size, while the motion pattern of objects is variable in different scenes. As shown in Fig. 3, objects with a fast-

moving speed are far apart across the BEV feature maps. To deal with this issue, we propose to enlarge the receptive field through spatial down-sampling by inserting convolutions of stride 2 at intervals, allowing it to capture a wide range of motion patterns. The above process can be formulated as:

$$\mathcal{Y} = \text{Convs}([\mathcal{X}_{t-1}; \mathcal{X}_t]), \quad (2)$$

where  $\text{Convs}$  denotes the convolutional blocks in BMM and  $[\cdot]$  denotes the concatenation operator.  $\mathcal{Y} \in \mathbb{R}^{H' \times W' \times C'}$ , where  $H'$ ,  $W'$ , and  $C'$  denote the spatial dimension and the number of feature channels, respectively.

### D. Distribution-aware Regression

Different from the existing two-stage point-to-box prediction head [4], [8], [15], which contains two parts of proposals generation and proposal-wise scores prediction, we propose a one-stage post-processing-free prediction head consisting of only a global max-pooling layer and an MLP, *i.e.*,

$$\mathcal{M} = \text{MLP}(\text{Pool}(\mathcal{Y})), \quad (3)$$

where  $\mathcal{M} \in \mathbb{R}^8$  denotes the expectation of the target translation and yaw offsets  $\bar{u} \in \mathbb{R}^4$  and their standard deviation  $\sigma \in \mathbb{R}^4$ , in contrast to prior methods that solely regress the deterministic target motion  $u$ . By applying the predicted translation to the last state of the target, we can localize the target in the current frame. Note that the standard deviation  $\sigma$  enables dynamic optimization during training while being removed in the inference phase, as elaborated below.

The difference in sizes, moving patterns, and sparsity degrees among the tracked targets poses great challenges to existing trackers. To address this issue, we propose a novel distribution-aware regression strategy for tracking, which constructs the likelihood function with the learned underlying distributions adapted to distinct targets. In this way, the model

TABLE I: Comparisons with state-of-the-art methods on KITTI dataset. Success/Precision are used for evaluation. **Bold** and underline denote the best and the second-best scores, respectively.

Method	Source	Car (6424)	Pedestrian (6088)	Van (1248)	Cyclist (308)	Mean by Class	Mean (14068)
SC3D	CVPR19	41.3 / 57.9	18.2 / 37.8	40.4 / 47.0	41.5 / 70.4	35.4 / 53.3	31.2 / 48.5
P2B	CVPR20	56.2 / 72.8	28.7 / 49.6	40.8 / 48.4	32.1 / 44.7	39.5 / 53.9	42.4 / 60.0
BAT	ICCV21	60.5 / 77.7	42.1 / 70.1	52.4 / 67.0	33.7 / 45.4	47.2 / 65.1	51.2 / 72.8
V2B	NIPS21	70.5 / 81.3	48.3 / 73.5	50.1 / 58.0	40.8 / 49.7	52.4 / 65.6	58.4 / 75.2
PTTR	CVPR22	65.2 / 77.4	50.9 / 81.6	52.5 / 61.8	65.1 / 90.5	58.4 / 77.8	57.9 / 78.1
STNet	ECCV22	72.1 / 84.0	49.9 / 77.2	58.0 / 70.6	73.5 / 93.7	63.4 / 81.4	61.3 / 80.1
M2-Track	CVPR22	65.5 / 80.8	61.5 / 88.2	53.8 / 70.7	73.2 / 93.5	63.5 / 83.3	62.9 / 83.4
GLT-T	AAAI23	68.2 / 82.1	52.4 / 78.8	52.6 / 62.9	68.9 / 92.1	60.5 / 79.0	60.1 / 79.3
OSP2B	IJCAI23	67.5 / 82.3	53.6 / 85.1	56.3 / 66.2	65.6 / 90.5	60.8 / 81.0	60.5 / 82.3
CXTrack	CVPR23	69.1 / 81.6	67.0 / 91.5	60.0 / 71.8	74.2 / 94.3	67.6 / 84.8	67.5 / 85.3
SyncTrack	ICCV23	73.3 / 85.0	54.7 / 80.5	60.3 / 70.0	73.1 / 93.8	65.4 / 82.3	64.1 / 81.9
MBPTrack	ICCV23	<u>73.4 / 84.8</u>	<u>68.6 / 93.9</u>	<u>61.3 / 72.7</u>	<u>76.7 / 94.3</u>	<u>70.0 / 86.4</u>	<u>70.3 / 87.9</u>
BEVTrack	Ours	<b>74.9 / 86.5</b>	<b>69.5 / 94.3</b>	<b>66.0 / 77.2</b>	<b>77.0 / 94.7</b>	<b>71.9 / 88.2</b>	<b>71.8 / 89.2</b>
Improvement	-	<u>↑1.5 / ↑1.5</u>	<u>↑0.9 / ↑0.4</u>	<u>↑4.7 / ↑4.5</u>	<u>↑0.3 / ↑0.4</u>	<u>↑1.9 / ↑1.8</u>	<u>↑1.5 / ↑1.3</u>

can adaptively handle targets with different attributes, thus improving tracking performance.

Following [61], we model the distribution of the target motion  $u \sim P(u)$  with reparameterization, which assumes that objects belonging to the same category share the same density function family, but with different mean and variance. Specifically,  $P(u)$  can be obtained by scaling and shifting  $z$  from a zero-mean distribution  $z \sim P_Z(z)$  with transformation function  $u = \bar{u} + \sigma \cdot z$ , where  $\bar{u}$  denotes the expectation of the target translation offsets and  $\sigma$  denotes the scale factor of the distribution.  $P_Z(z)$  can be modeled by a normalizing flow model (e.g., real NVP [62]). Given this transformation function, the density function of  $P(u)$  can be calculated as:

$$\log P(u) = \log P_Z(z) - \log \sigma. \quad (4)$$

In this work, we employ residual log-likelihood estimation in [61] to estimate the above parameters, which factorizes the distribution  $P_Z(z)$  into one prior distribution  $Q_Z(z)$  (e.g., Laplacian distribution or Gaussian distribution) and one learned distribution  $G_Z(z | \theta)$ . To maximize the likelihood in Eq. (4), we can minimize the following loss:

$$\mathcal{L} = -\log Q_Z(\hat{z}) - \log G_Z(\hat{z} | \theta) + \log \sigma. \quad (5)$$

Here,  $\hat{z} = (\hat{u} - \bar{u})/\sigma$ ,  $\hat{u}$  is the ground truth translation offsets.

### E. Implementation Details

In our paper, we use 4 sparse convolution blocks with {16, 32, 64, 128} channels as the Siamese backbone. We adopt RealNVP [62] to learn the underlying residual log-likelihood. The RealNVP model is fast and lightweight. We adopt 3 blocks with 64 channels for the RealNVP design, while each block consists of 3 fully connected (FC) layers and each FC layer is followed by a Leaky-RELU [63] layer.

Our BEVTrack can be trained in an end-to-end manner. We train it on 2 NVIDIA GTX 4090 GPUs for 160 epochs using the AdamW optimizer with a learning rate of 1e-4. We use a batch size of 256 and a weight decay of 1e-5. For data augmentations, we adopt common schemes including random flipping, random rotation, and random translation during the training. The loss function is a single regression loss.

## IV. EXPERIMENT

### A. Experimental Settings

a) *Datasets*: We validate the effectiveness of BEVTrack on three widely-used challenging datasets: KITTI [20], NuScenes [21], and Waymo Open Dataset (WOD) [22]. KITTI contains 21 video sequences for training and 29 video sequences for testing. We follow previous work [4] to split the training set into train/val/test splits due to the inaccessibility of the labels of the test set. NuScenes contains 1,000 scenes, which are divided into 700/150/150 scenes for train/val/test. Following the implementation in [6], we compare with the previous methods on five categories including *Car*, *Pedestrian*, *Truck*, *Trailer*, and *Bus*. WOD includes 1150 scenes with 798 for training, 202 for validation, and 150 for testing. Following M2-Track [5], We conduct training and testing respectively on the training and validation set.

b) *Evaluation Metrics*: Following [4], we adopt Success and Precision defined in one pass evaluation (OPE) [64] as the evaluation metrics. Success denotes the Area Under Curve (AUC) for the plot showing the ratio of frames where the Intersection Over Union (IoU) between the predicted box and the ground truth is larger than a threshold, ranging from 0 to 1, while Precision denotes the AUC for the plot showing the ratio of frames where the distance between their centers is within a threshold, ranging from 0 to 2 meters.

### B. Comparison with State-of-the-art Methods

a) *Results on KITTI*: We present a comprehensive comparison of BEVTrack with the previous state-of-the-art approaches on KITTI, namely SC3D [29], P2B [4], BAT [6], V2B [38], PTTR [8], GLT-T [31], OSP2B [7], STNet [15], M2-Track [5], CXTrack [11], SyncTrack [33], and MBPTrack [34]. As shown in Tab. I, BEVTrack surpasses current tracking methods with a significant improvement across all categories on KITTI in *Success* and *Precision* metrics. We also visualize the tracking results on four KITTI categories for qualitative comparisons. As shown in Fig. 4, BEVTrack generates more robust and accurate tracking predictions.

For a more comprehensive evaluation of effectiveness in challenging scenarios, we present results from various methods

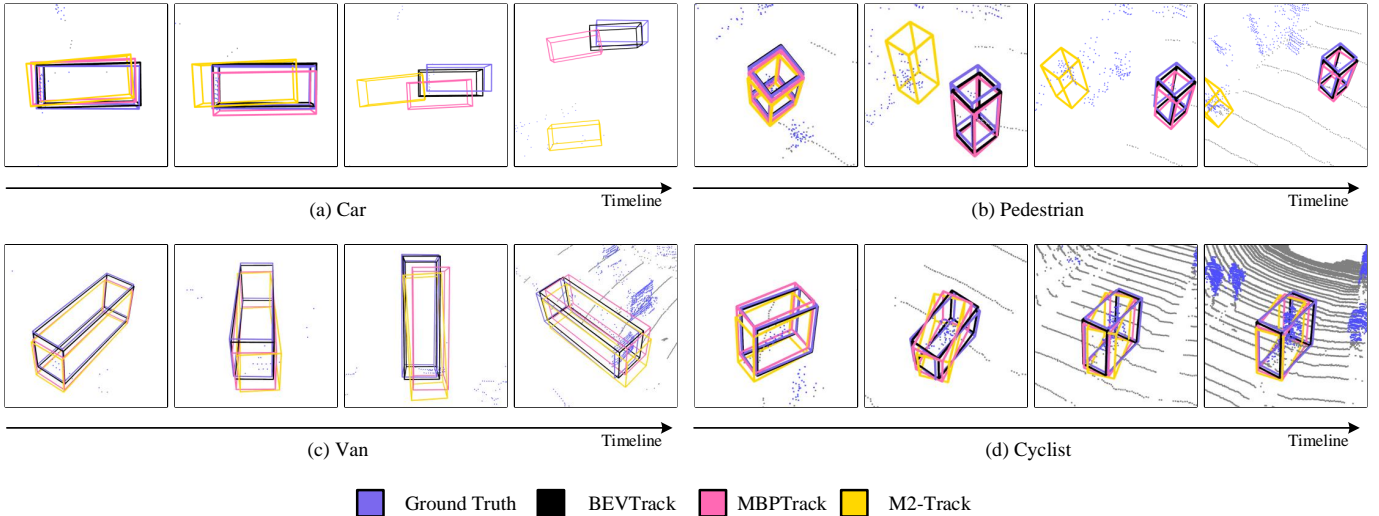


Fig. 4: Visualization results on different KITTI categories: (a) Car; (b) Pedestrian; (c) Van; (d) Cyclist.

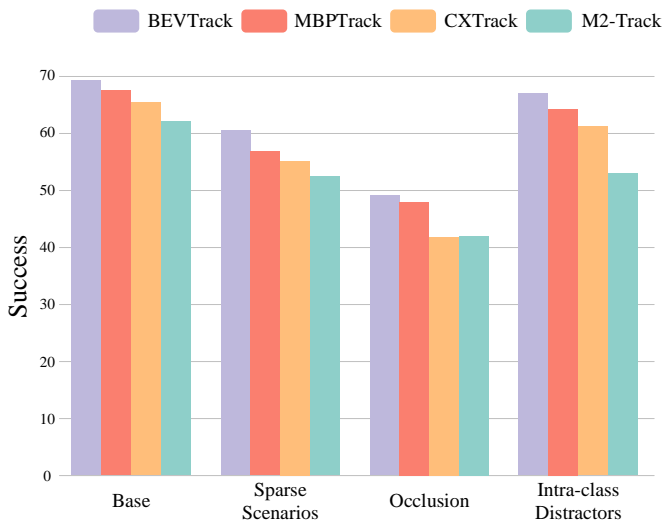


Fig. 5: Robustness under different challenging scenes on KITTI Pedestrian category.

in cases characterized by sparse scenarios, occlusion, and intra-class distractors. To verify the effectiveness in sparse scenarios, we follow V2B [38] to select sparse scenes for evaluation according to the number of points lying in the target bounding boxes in the test set. For analysis of the impact of intra-class distractors, we pick out scenes that contain Pedestrian distractors close to the target from the KITTI test split. For the occlusion situations, we filter out scenes of occlusion scores less than one in the KITTI test set.

As shown in Fig. 5, each column from left to right represents the cases of base setting, sparse scenarios, occlusion, and intra-class distractors respectively on the Pedestrian category of the KITTI dataset. Our proposed BEVTrack models the motion of both targets and intra-class distractors using BEV features, thereby harnessing contextual and spatial information effectively. This approach results in improved target localization accuracy, particularly in challenging scenarios.

**b) Results on Nuscenes:** NuScenes poses a more formidable challenge for the 3D SOT task compared to KITTI, primarily attributable to its larger data volumes and sparser annotations (2Hz for NuScenes versus 10Hz for KITTI and Waymo Open Dataset). Subsequently, following the methodology established by M2-Track, we perform a comparative evaluation on the NuScenes dataset against prior methodologies, namely SC3D [29], P2B [4], PTT [30], BAT [6], GLT-T [31], PTTR [8], M2Track [5], and MBPTrack [34]. As shown in Tab. II, our method achieves a consistent and large performance gain compared with the previous state-of-the-art method, MBPTrack. BEVTrack exhibits superior performance over methods reliant on appearance matching or segmentation, especially in datasets like NuScenes with sparser point clouds. We also visualize the tracking results on four NuScenes categories for qualitative comparisons. As shown in Fig. 6, when there are distractors around the target, conventional approaches tend to drift towards these distractors as a consequence of excessive dependence on appearance matching or segmentation. In contrast, BEVTrack can track point cloud objects more accurately and robustly.

**c) Results on WOD:** WOD dataset presents greater challenges compared to KITTI and NuScenes due to its larger data volumes and complexities. Following M2-Track [5], we conduct training and testing on the respective training and validation sets. We consider trackers that report results under this setting as competitors, including P2B [4], BAT [6], and M2-Track [5]. As illustrated in Tab. III, BEVTrack consistently outperforms all competitors on average, particularly excelling in the *Vehicle* category. Remarkably, BEVTrack, with its simple design, demonstrates even greater potential on this large dataset.

**d) Comparison with MOT Approaches:** Furthermore, we present a comparison of BEVTrack on the KITTI SOT benchmark with the state-of-the-art 3D multi-object tracking (MOT) methods, *i.e.*, AB3D [54] and PC3T [57]. To ensure fairness, we initialize AB3D and PC3T with ground truth bounding boxes in the initial frame instead of relying on

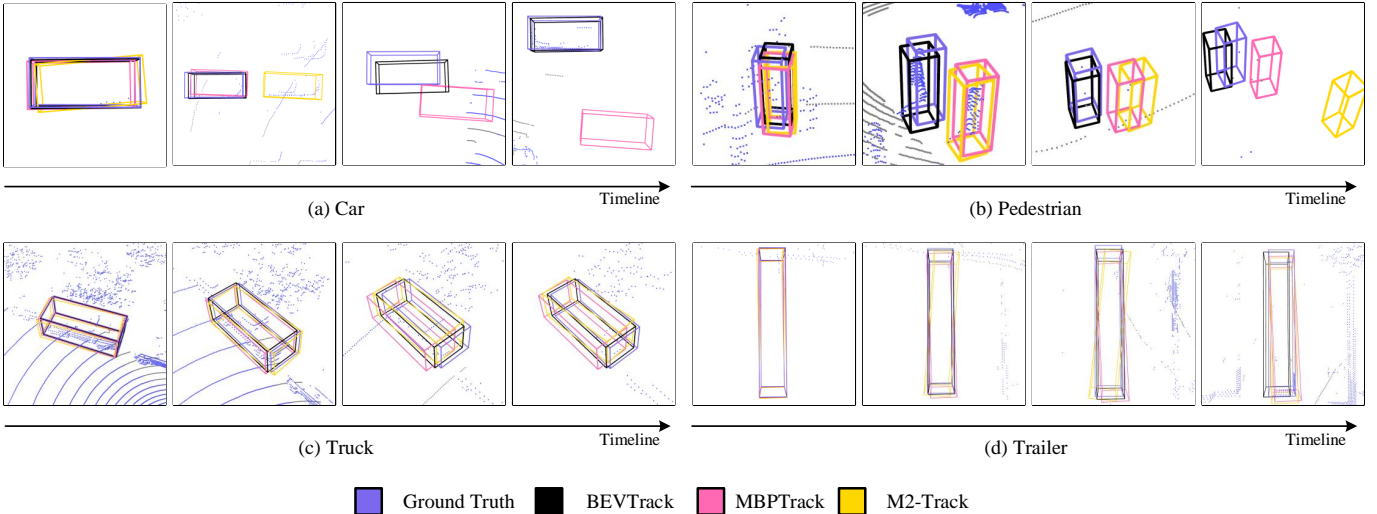


Fig. 6: Visualization results on different NuScenes categories: (a) Car; (b) Pedestrian; (c) Truck; (d) Trailer.

TABLE II: Comparisons with the state-of-the-art methods on NuScenes dataset.

Method	Car (64,159)	Pedestrian (33,227)	Truck (13,587)	Trailer (3,352)	Bus (2,953)	Mean by Class	Mean (117,278)
SC3D	22.31 / 21.93	11.29 / 12.65	35.28 / 28.12	35.28 / 28.12	29.35 / 24.08	25.78 / 22.90	20.70 / 20.20
P2B	38.81 / 43.18	28.39 / 52.24	48.96 / 40.05	48.96 / 40.05	32.95 / 27.41	38.41 / 40.90	36.48 / 45.08
PTT	41.22 / 45.26	19.33 / 32.03	50.23 / 48.56	51.70 / 46.50	39.40 / 36.70	40.38 / 41.81	36.33 / 41.72
BAT	40.73 / 43.29	28.83 / 53.32	52.59 / 44.89	52.59 / 44.89	35.44 / 28.01	40.59 / 42.42	38.10 / 45.71
GLT-T	48.52 / 54.29	31.74 / 56.49	52.74 / 51.43	57.60 / 52.01	44.55 / 40.69	47.03 / 50.98	44.42 / 54.33
PTTR	51.89 / 58.61	29.90 / 45.09	45.30 / 44.74	45.87 / 38.36	43.14 / 37.74	43.22 / 44.91	44.50 / 52.07
M2-Track	55.85 / 65.09	32.10 / 60.92	57.36 / 59.54	57.61 / 58.26	51.39 / 51.44	50.86 / 59.05	49.23 / 62.73
MBPTrack	62.47 / 70.41	45.32 / 74.03	62.18 / 63.31	65.14 / 61.33	55.41 / 51.76	58.10 / 64.17	57.48 / 69.88
BEVTrack	<b>64.31 / 71.14</b>	<b>46.28 / 76.77</b>	<b>66.83 / 67.04</b>	<b>74.54 / 71.62</b>	<b>61.09 / 56.68</b>	<b>62.61 / 68.65</b>	<b>59.71 / 71.19</b>
Improvement	$\uparrow 1.84$ / $\uparrow 0.73$	$\uparrow 0.96$ / $\uparrow 2.74$	$\uparrow 4.65$ / $\uparrow 3.73$	$\uparrow 9.40$ / $\uparrow 10.29$	$\uparrow 5.68$ / $\uparrow 4.92$	$\uparrow 4.51$ / $\uparrow 4.48$	$\uparrow 2.23$ / $\uparrow 1.31$

TABLE III: Comparisons with the state-of-the-art methods on Waymo Open Dataset.

Method	Vehicle 1,057,651	Pedestrian 510,533	Mean 1,568,184
P2B	28.32 / 35.41	15.60 / 29.56	24.18 / 33.51
BAT	35.62 / 44.15	22.05 / 36.79	31.20 / 41.75
M2-Track	43.62 / 61.64	42.10 / 67.31	43.13 / 63.48
BEVTrack	<b>70.05 / 80.05</b>	<b>45.93 / 72.41</b>	<b>62.20 / 77.56</b>
Improvement	$\uparrow 26.43$ / $\uparrow 18.41$	$\uparrow 3.83$ / $\uparrow 5.10$	$\uparrow 19.07$ / $\uparrow 14.08$

their detector outputs. Consequently, each MOT task can be decomposed into several SOT tasks. We evaluate the tracking results of these MOT methods using 3D SOT metrics. The results, as presented in Tab. IV, demonstrate that BEVTrack significantly outperforms state-of-the-art 3D MOT methods. Since MOT relies on the pre-detection, tracklets will be destroyed when detections are missed for multiple frames, resulting in tracking failure. Meanwhile, the nature of MOT, which encompasses all objects in scenes and depends on detectors for object localization, prevents it from achieving the precision of SOT for individual objects.

*e) Inference Speed:* We analyze the efficiency of BEVTrack in Tab. V. It can be observed that BEVTrack is lightweight with only 0.76G FLOPs and 13.8M parameters. The simple convolutional architecture employed by BEVTrack ensures real-time inference at an impressive speed of 201 FPS

TABLE IV: Comparison with MOT methods on KITTI dataset.

Class	AB3D [54]	PC3T [57]	BEVTrack
Car	37.5 / 42.3	51.9 / 59.2	74.9 / 86.5
Ped	17.6 / 27.3	23.6 / 34.1	69.5 / 94.3

TABLE V: Efficiency analysis.

Method	Params	FLOPs	Infer time
CXTrack	18.3M	4.63G	16.4ms
MBPTrack	7.4M	2.88G	11.7ms
BEVTrack	13.8M	0.76G	4.98ms

on a single NVIDIA GTX 4090 GPU, which is 2.34 times faster than the previously leading method, MBPTrack [34]. The simplicity of BEVTrack’s pipeline facilitates flexible adjustments in model size by incorporating advanced backbones or devising more effective BMM modules to further enhance performance. This paper aims to establish a baseline model for 3D SOT and favors a lightweight structure to strike a balance between performance and efficiency. The exploration of more effective architectural designs remains a potential avenue for future research.

TABLE VI: Ablation study of BEV Feature Extraction Method.

Methods	Latency	Car	Pedestrian	Van	Cyclist	Mean
Pre-BEV	4.98 ms	74.9 / 86.5	69.5 / 94.3	66.0 / 77.2	77.0 / 94.7	71.8 / 89.2
Post-BEV	1.66 ms	72.2 / 85.0	67.2 / 93.8	62.7 / 74.6	78.1 / 94.7	69.3 / 88.1

TABLE VII: Ablation study of the BMM module.

ratio	Car	Pedestrian	Van	Cyclist	Mean
1×	71.7 / 81.5	65.3 / 91.2	65.5 / 76.3	76.0 / 94.0	68.5 / 85.5
2×	72.1 / 83.0	63.2 / 91.4	65.8 / 75.8	75.3 / 93.7	67.8 / 86.2
4×	<b>74.9 / 86.5</b>	<b>69.5 / 94.3</b>	66.0 / 77.2	<b>77.0 / 94.7</b>	<b>71.8 / 89.2</b>
8×	74.7 / <b>86.8</b>	68.1 / 93.7	<b>66.5 / 77.4</b>	75.2 / 93.7	71.1 / 89.1

TABLE VIII: Ablation study of the regression strategy. ‘‘G’’ refers to regress with Gaussian assumption, ‘‘L’’ refers to regress with Laplacian assumption and ‘‘D’’ refers to regress with distribution-aware tracking strategy.

	Car	Pedestrian	Van	Cyclist	Mean
G	68.0 / 80.8	59.8 / 88.6	61.8 / 71.9	69.8 / 92.4	63.9 / 83.6
L	69.2 / 81.8	64.2 / 90.7	58.9 / 72.2	73.2 / 93.5	66.2 / 85.1
D	<b>74.9 / 86.5</b>	<b>69.5 / 94.3</b>	<b>66.0 / 77.2</b>	<b>77.0 / 94.7</b>	<b>71.8 / 89.2</b>

### C. Ablation Studies

To validate the effectiveness of the design choice in bev-Track, we conduct ablation studies on the KITTI dataset.

a) **BEV Features Extraction:** According to the order of feature extraction and BEV feature transformation, there are mainly two branches to convert point cloud data into BEV representation, *i.e.*, Pre-BEV which extracts point cloud features in 3D space before converting point cloud data into BEV representation, and Post-BEV which extracts BEV features in BEV space directly. We make ablations on the backbone of 3D sparse CNN and 2D dense CNN, corresponding to the Pre-BEV and Post-BEV respectively, in Tab. VI. Pre-BEV paradigm employing 3D sparse CNN in the backbone yields accurate results but incurs high latency. This configuration serves as the default setting for BEVTrack. In contrast, when utilizing a 2D dense CNN as the backbone network with an equivalent number of layers and channels compared to the 3D counterpart, it achieves superior efficiency. Despite the performance degradation, it consistently outperforms the previous competitive method, *e.g.*, M2Track, across all categories. It could be an alternative choice for our BEVTrack when favoring high computational efficiency.

b) **Design Choice of the BMM Module:** As detailed in Sec. III-C, for tracking targets with diverse motion patterns, the motion modeling module necessitates sufficient receptive fields. Our approach enlarges receptive fields through spatial down-sampling of features, but sacrificing fine-grained detail information due to the resulting smaller feature maps. In order to reach a balance between sufficient receptive fields and fine-grained detail information, we compare the tracking accuracy when motion modeling is performed under different down-sampling ratios. For a fair comparison, the number of convolutional layers is the same in different settings. The results in Tab. VII demonstrate that the 4× down-sampling configuration yields the best performance. Consequently, we adopt this configuration as the default setting.

TABLE IX: Ablation study of the fusion method in BMM.

operation	Car	Pedestrian	Van	Cyclist	Mean
cat(c)	<b>74.9 / 86.5</b>	<b>69.5 / 94.3</b>	<b>66.0 / 77.2</b>	<b>77.0 / 94.7</b>	<b>71.8 / 89.2</b>
sum(+)	69.5 / 82.4	60.1 / 85.3	63.6 / 75.2	76.3 / 94.2	65.1 / 83.3
mul(×)	61.6 / 71.4	57.2 / 84.8	65.2 / 76.2	74.2 / 94.2	60.3 / 78.1
sub(-)	70.1 / 80.5	61.0 / 85.6	63.2 / 75.5	76.5 / 94.4	65.7 / 82.6

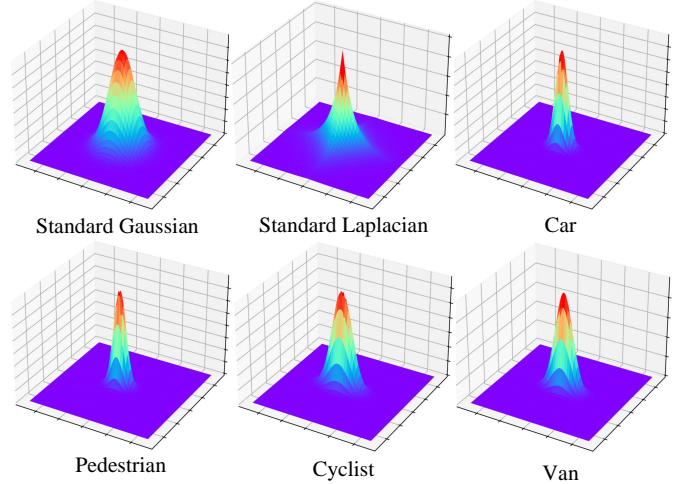


Fig. 7: Visualization of the learned distributions.

c) **Distribution-aware Regression:** To examine how the assumption of the output distribution affects the tracking performance, we compare the tracking results of utilizing different density functions as well as the proposed distribution-aware regression strategy. The Laplacian distribution and Gaussian distribution will degenerate to standard  $l_1$  and  $l_2$  loss if they are assumed to have constant variances. As shown in Tab. VIII, the distribution-aware regression approach achieves better performance than the regression with  $l_1$  or  $l_2$  loss, which demonstrates the importance of learning the actual distribution. We visualize the distributions learned by normalizing flow across different categories in Fig. 7. The learned distribution has a sharper peak than the Gaussian distribution and a smoother edge than the Laplacian distribution, while this difference demonstrates the importance of the distribution-aware optimization scheme. Furthermore, there are also differences between the learned distributions across different categories, implying that assuming all categories conform to a fixed Laplacian or Gaussian distribution may be not optimal.

d) **Fusion Method in BMM:** Feature fusion propagates the target cues into the search area, which is a critical aspect of the 3D SOT task. We investigate various fusion techniques: concatenation (denoted as ‘cat (c)’), summation (‘sum (+)’), multiplication (‘mul (×)’), and subtraction (‘sub (-)’). As shown in Tab. IX, the concatenation operation yields the best performance across all categories, outperforming others with a maximum improvement in precision and success of 11.1% and

11.5%, respectively. Consequently, we select concatenation as the default setting. It shows that an appropriate fusion method is important for tracking, and we believe that our method could benefit from more research progress in this direction.

## V. CONCLUSION

This paper introduces BEVTrack, a simple yet strong baseline for 3D single object tracking (SOT). BEVTrack performs tracking within the Bird’s-Eye View representation, thereby effectively exploiting spatial information and capturing motion cues. Additionally, we propose a distribution-aware regression strategy that learns the actual distribution adapted to targets possessing diverse attributes, providing accurate guidance for tracking. Comprehensive experiments conducted on widely recognized benchmarks underscore BEVTrack’s efficacy, establishing its superiority over state-of-the-art tracking methods. Furthermore, it achieves a high inference speed of about 200 FPS. We hope this study could provide valuable insights to the tracking community and inspire further research on BEV-based 3D SOT methods.

Limitation: One limitation of BEVTrack is that, despite being robust to typical challenging scenarios, it tends to drift to background points when point clouds are extremely sparse. A promising solution is to incorporate multi-modal information. On the one hand, image data can complement the sparsity of point cloud data. On the other hand, BEV, as the unified representation for multi-modal fusion [65]–[67], adeptly preserves semantic information from cameras and geometric information from LiDAR. We envision that BEVTrack can serve as an inspiration for further research into multi-modal fusion methodologies for SOT.

## REFERENCES

- [1] T. Yin, X. Zhou, and P. Krahenbuhl, “Center-based 3d object detection and tracking,” in *Proceedings of the IEEE/CVF Conference on Computer Vision and Pattern Recognition*, 2021, pp. 11 784–11 793. **1**
- [2] Y. Cai, L. Dai, H. Wang, and Z. Li, “Multi-target pan-class intrinsic relevance driven model for improving semantic segmentation in autonomous driving,” *IEEE Transactions on Image Processing*, vol. 30, pp. 9069–9084, 2021. **1**
- [3] H.-k. Chiu, A. Prioletti, J. Li, and J. Bohg, “Probabilistic 3d multi-object tracking for autonomous driving,” *arXiv preprint arXiv:2001.05673*, 2020. **1**
- [4] H. Qi, C. Feng, Z. Cao, F. Zhao, and Y. Xiao, “P2b: point-to-box network for 3d object tracking in point clouds,” in *Proceedings of the IEEE/CVF Conference on Computer Vision and Pattern Recognition*, 2020, pp. 6329–6338. **1, 2, 3, 4, 5, 6**
- [5] C. Zheng, X. Yan, H. Zhang, B. Wang, S. Cheng, S. Cui, and Z. Li, “Beyond 3d siamese tracking: A motion-centric paradigm for 3d single object tracking in point clouds,” in *Proceedings of the IEEE/CVF International Conference on Computer Vision*, 2022, pp. 8111–8120. **1, 2, 4, 5, 6**
- [6] C. Zheng, X. Yan, J. Gao, W. Zhao, W. Zhang, Z. Li, and S. Cui, “Box-aware feature enhancement for single object tracking on point clouds,” in *Proceedings of the IEEE/CVF International Conference on Computer Vision*, 2021, pp. 13 199–13 208. **1, 2, 5, 6**
- [7] J. Nie, Z. He, Y. Yang, Z. Bao, M. Gao, and J. Zhang, “Osp2b: One-stage point-to-box network for 3d siamese tracking,” in *Proceedings of the International Joint Conference on Artificial Intelligence*, 2023. **1, 5**
- [8] C. Zhou, Z. Luo, Y. Luo, T. Liu, L. Pan, Z. Cai, H. Zhao, and S. Lu, “Ptr: Relational 3d point cloud object tracking with transformer,” in *Proceedings of the IEEE/CVF Conference on Computer Vision and Pattern Recognition*, 2022, pp. 8531–8540. **1, 2, 4, 5, 6**
- [9] C. R. Qi, L. Yi, H. Su, and L. J. Guibas, “Pointnet++: Deep hierarchical feature learning on point sets in a metric space,” *Advances in Neural Information Processing Systems*, vol. 30, 2017. **1, 4**
- [10] Y. Wang, Y. Sun, Z. Liu, S. E. Sarma, M. M. Bronstein, and J. M. Solomon, “Dynamic graph cnn for learning on point clouds,” *ACM Transactions on Graphics*, p. 1–12, 2019. **1, 4**
- [11] T.-X. Xu, Y.-C. Guo, Y.-K. Lai, and S.-H. Zhang, “Cxtrack: Improving 3d point cloud tracking with contextual information,” in *Proceedings of the IEEE/CVF Conference on Computer Vision and Pattern Recognition*, 2023, pp. 1084–1093. **1, 2, 4, 5**
- [12] C. R. Qi, O. Litany, K. He, and L. J. Guibas, “Deep hough voting for 3d object detection in point clouds,” in *Proceedings of the IEEE/CVF International Conference on Computer Vision*, 2019, pp. 9277–9286. **1, 2**
- [13] Z. Fang, S. Zhou, Y. Cui, and S. Scherer, “3d-siamrpn: An end-to-end learning method for real-time 3d single object tracking using raw point cloud,” *IEEE Sensors Journal*, p. 4995–5011, 2021. **1**
- [14] C. R. Qi, H. Su, K. Mo, and L. J. Guibas, “Pointnet: Deep learning on point sets for 3d classification and segmentation,” in *Proceedings of the IEEE Conference on Computer Vision and Pattern Recognition*, 2017, pp. 652–660. **1, 2, 4**
- [15] L. Hui, L. Wang, L. Tang, K. Lan, J. Xie, and J. Yang, “3d siamese transformer network for single object tracking on point clouds,” in *Proceedings of the European Conference on Computer Vision*, 2022, pp. 293–310. **1, 2, 4, 5**
- [16] J. Nie, Z. He, Y. Yang, X. Lv, M. Gao, and J. Zhang, “Glt-t++: Global-local transformer for 3d siamese tracking with ranking loss,” *arXiv preprint arXiv:2304.00242*, 2023. **1**
- [17] Y. Zhou and O. Tuzel, “Voxelnet: End-to-end learning for point cloud based 3d object detection,” in *Proceedings of the IEEE/CVF Conference on Computer Vision and Pattern Recognition*, 2018, pp. 4490–4499. **1, 2, 3, 4**
- [18] F. Duffhauß and S. A. Baur, “Pillarflownet: A real-time deep multitask network for lidar-based 3d object detection and scene flow estimation,” in *2020 IEEE/RSJ International Conference on Intelligent Robots and Systems (IROS)*. IEEE, 2020, pp. 10 734–10 741. **2**
- [19] Y. Yan, Y. Mao, and B. Li, “Second: Sparsely embedded convolutional detection,” *Sensors*, vol. 18, no. 10, p. 3337, 2018. **2**
- [20] A. Geiger, P. Lenz, and R. Urtasun, “Are we ready for autonomous driving? the kitti vision benchmark suite,” in *Proceedings of the IEEE Conference on Computer Vision and Pattern Recognition*, 2012, pp. 3354–3361. **2, 5**
- [21] H. Caesar, V. Bankiti, A. H. Lang, S. Vora, V. E. Liong, Q. Xu, A. Krishnan, Y. Pan, G. Baldan, and O. Beijbom, “Nuscenes: A multimodal dataset for autonomous driving,” in *Proceedings of the IEEE/CVF Conference on Computer Vision and Pattern Recognition*, 2020, pp. 11 621–11 631. **2, 5**
- [22] P. Sun, H. Kretzschmar, X. Dotiwalla, A. Chouard, V. Patnaik, P. Tsui, J. Guo, Y. Zhou, Y. Chai, B. Caine, V. Vasudevan, W. Han, J. Ngiam, H. Zhao, A. Timofeev, S. Ettinger, M. Krivokon, A. Gao, A. Joshi, Y. Zhang, J. Shlens, Z. Chen, and D. Anguelov, “Scalability in perception for autonomous driving: waymo open dataset,” in *Proceedings of the IEEE/CVF Conference on Computer Vision and Pattern Recognition*, 2020, pp. 2446–2454. **2, 5**
- [23] A. Pieropan, N. Bergström, M. Ishikawa, and H. Kjellström, “Robust 3d tracking of unknown objects,” in *Proceedings of the IEEE International Conference on Robotics and Automation*, 2015, pp. 2410–2417. **2**
- [24] L. Spinello, K. Arras, R. Triebel, and R. Siegwart, “A layered approach to people detection in 3d range data,” in *Proceedings of the AAAI Conference on Artificial Intelligence*, 2010, pp. 1625–1630. **2**
- [25] M. H. Abdelpakey and M. S. Shehata, “Dp-siam: Dynamic policy siamese network for robust object tracking,” *IEEE Transactions on Image Processing*, vol. 29, pp. 1479–1492, 2019. **2**
- [26] S. Chan, J. Tao, X. Zhou, C. Bai, and X. Zhang, “Siamese implicit region proposal network with compound attention for visual tracking,” *IEEE Transactions on Image Processing*, vol. 31, pp. 1882–1894, 2022. **2**
- [27] T. Xu, Z. Feng, X.-J. Wu, and J. Kittler, “Toward robust visual object tracking with independent target-agnostic detection and effective siamese cross-task interaction,” *IEEE Transactions on Image Processing*, vol. 32, pp. 1541–1554, 2023. **2**
- [28] Z. Liu, X. Wang, Y. Zhong, M. Shu, and C. Sun, “Siamhyper: Learning a hyperspectral object tracker from an rgb-based tracker,” *IEEE Transactions on Image Processing*, vol. 31, pp. 7116–7129, 2022. **2**
- [29] S. Giancola, J. Zarzar, and B. Ghanem, “Leveraging shape completion for 3d siamese tracking,” in *Proceedings of the IEEE/CVF Conference on Computer Vision and Pattern Recognition*, 2019, pp. 1359–1368. **2, 5, 6**
- [30] J. Shan, S. Zhou, Z. Fang, and Y. Cui, “Ptt: Point-track-transformer module for 3d single object tracking in point clouds,” in *Proceedings*

- of the *IEEE/RSJ International Conference on Intelligent Robots and Systems*, 2021, pp. 1310–1316. **2, 6**
- [31] J. Nie, Z. He, Y. Yang, M. Gao, and J. Zhang, “Glt-t: Global-local transformer voting for 3d single object tracking in point clouds,” in *Proceedings of the AAAI Conference on Artificial Intelligence*, 2023, pp. 1957–1965. **2, 5, 6**
- [32] A. Vaswani, N. Shazeer, N. Parmar, J. Uszkoreit, L. Jones, A. Gomez, L. Kaiser, and I. Polosukhin, “Attention is all you need,” *Advances in Neural Information Processing Systems*, vol. 30, 2017. **2**
- [33] T. Ma, M. Wang, J. Xiao, H. Wu, and Y. Liu, “Synchronize feature extracting and matching: A single branch framework for 3d object tracking,” in *Proceedings of the IEEE/CVF International Conference on Computer Vision*, 2023, pp. 9953–9963. **2, 5**
- [34] T.-X. Xu, Y.-C. Guo, Y.-K. Lai, and S.-H. Zhang, “Mbptrack: Improving 3d point cloud tracking with memory networks and box priors,” in *Proceedings of the IEEE/CVF International Conference on Computer Vision*, 2023, pp. 9911–9920. **2, 5, 6, 7**
- [35] C. Zheng, X. Yan, H. Zhang, B. Wang, S. Cheng, S. Cui, and Z. Li, “An effective motion-centric paradigm for 3d single object tracking in point clouds,” *IEEE Transactions on Pattern Analysis and Machine Intelligence*, 2023. **2**
- [36] J. Zarzar, S. Giancola, and B. Ghanem, “Efficient bird eye view proposals for 3d siamese tracking,” *arXiv preprint arXiv:1903.10168*, 2019. **2**
- [37] Y. Cui, Z. Fang, J. Shan, Z. Gu, and S. Zhou, “3d object tracking with transformer,” *arXiv preprint arXiv:2110.14921*, 2021. **2**
- [38] L. Hui, L. Wang, M. Cheng, J. Xie, and J. Yang, “3d siamese voxel-to-bev tracker for sparse point clouds,” *Advances in Neural Information Processing Systems*, vol. 34, pp. 28 714–28 727, 2021. **2, 5, 6**
- [39] Y. Cui, Z. Li, and Z. Fang, “Sstracker: Spatio-temporal tracker for 3d single object tracking,” *IEEE Robotics and Automation Letters*, 2023. **2**
- [40] T. Yin, X. Zhou, and P. Krahenbuhl, “Center-based 3d object detection and tracking,” in *Proceedings of the IEEE/CVF Conference on Computer Vision and Pattern Recognition*, 2021, pp. 11 784–11 793. **2, 3**
- [41] J. Deng, S. Shi, P. Li, W. Zhou, Y. Zhang, and H. Li, “Voxel r-cnn: Towards high performance voxel-based 3d object detection,” in *Proceedings of the AAAI conference on Artificial Intelligence*, vol. 35, no. 2, 2021, pp. 1201–1209. **2**
- [42] J. Mao, M. Niu, H. Bai, X. Liang, H. Xu, and C. Xu, “Pyramid r-cnn: Towards better performance and adaptability for 3d object detection,” in *Proceedings of the IEEE/CVF International Conference on Computer Vision*, 2021, pp. 2723–2732. **2**
- [43] S. Shi, C. Guo, L. Jiang, Z. Wang, J. Shi, X. Wang, and H. Li, “Pv-rnn: Point-voxel feature set abstraction for 3d object detection,” in *Proceedings of the IEEE/CVF Conference on Computer Vision and Pattern Recognition*, 2020, pp. 10 529–10 538. **2**
- [44] H. Yang, Z. Liu, X. Wu, W. Wang, W. Qian, X. He, and D. Cai, “Graph r-cnn: Towards accurate 3d object detection with semantic-decorated local graph,” in *European Conference on Computer Vision*. Springer, 2022, pp. 662–679. **2**
- [45] A. H. Lang, S. Vora, H. Caesar, L. Zhou, J. Yang, and O. Beijbom, “Pointpillars: Fast encoders for object detection from point clouds,” in *Proceedings of the IEEE/CVF Conference on Computer Vision and Pattern Recognition*, 2019, pp. 12 697–12 705. **2, 3**
- [46] K. Duan, S. Bai, L. Xie, H. Qi, Q. Huang, and Q. Tian, “Centernet: Keypoint triplets for object detection,” in *Proceedings of the IEEE/CVF International Conference on Computer Vision*, 2019, pp. 6569–6578. **2**
- [47] X. Zhou, V. Koltun, and P. Krähenbühl, *Tracking Objects as Points*, Jan 2020, p. 474–490. [Online]. Available: [http://dx.doi.org/10.1007/978-3-030-58548-8\\_28](http://dx.doi.org/10.1007/978-3-030-58548-8_28) **2**
- [48] H. Li, C. Sima, J. Dai, W. Wang, L. Lu, H. Wang, J. Zeng, Z. Li, J. Yang, H. Deng *et al.*, “Delving into the devils of bird’s-eye-view perception: A review, evaluation and recipe,” *IEEE Transactions on Pattern Analysis and Machine Intelligence*, 2023. **2**
- [49] Y. Chen, J. Liu, X. Zhang, X. Qi, and J. Jia, “Voxelnext: Fully sparse voxelnet for 3d object detection and tracking,” in *Proceedings of the IEEE/CVF Conference on Computer Vision and Pattern Recognition*, 2023, pp. 21 674–21 683. **3**
- [50] S. Shi, X. Wang, and H. Li, “Pointrcnn: 3d object proposal generation and detection from point cloud,” in *Proceedings of the IEEE/CVF Conference on Computer Vision and Pattern Recognition*, 2019, pp. 770–779. **3**
- [51] A. Bewley, Z. Ge, L. Ott, F. Ramos, and B. Upcroft, “Simple online and realtime tracking,” in *2016 IEEE International Conference on Image Processing (ICIP)*. IEEE, 2016, pp. 3464–3468. **3**
- [52] N. Wojke, A. Bewley, and D. Paulus, “Simple online and realtime tracking with a deep association metric,” in *2017 IEEE International Conference on Image Processing (ICIP)*. IEEE, 2017, pp. 3645–3649. **3**
- [53] T. Yin, X. Zhou, and P. Krahenbuhl, “Center-based 3d object detection and tracking,” in *Proceedings of the IEEE/CVF Conference on Computer Vision and Pattern Recognition*, 2021, pp. 11 784–11 793. **3**
- [54] X. Weng, J. Wang, D. Held, and K. Kitani, “3d multi-object tracking: A baseline and new evaluation metrics,” in *2020 IEEE/RSJ International Conference on Intelligent Robots and Systems (IROS)*, 2020, pp. 10 359–10 366. **3, 6, 7**
- [55] H.-k. Chiu, A. Prioletti, J. Li, and J. Bohg, “Probabilistic 3d multi-object tracking for autonomous driving,” *arXiv preprint arXiv:2001.05673*. **3**
- [56] M. Liang, B. Yang, W. Zeng, Y. Chen, R. Hu, S. Casas, and R. Urtasun, “Pnpnet: End-to-end perception and prediction with tracking in the loop,” in *Proceedings of the IEEE/CVF Conference on Computer Vision and Pattern Recognition*, 2020, pp. 11 553–11 562. **3**
- [57] H. Wu, W. Han, C. Wen, X. Li, and C. Wang, “3d multi-object tracking in point clouds based on prediction confidence-guided data association,” *IEEE Transactions on Intelligent Transportation Systems*, vol. 23, no. 6, pp. 5668–5677, 2021. **3, 6, 7**
- [58] C. Luo, X. Yang, and A. Yuille, “Exploring simple 3d multi-object tracking for autonomous driving,” in *Proceedings of the IEEE/CVF International Conference on Computer Vision*, 2021, pp. 10 488–10 497. **3**
- [59] B. Graham and L. Van der Maaten, “Submanifold sparse convolutional networks,” *arXiv preprint arXiv:1706.01307*, 2017. **4**
- [60] B. Graham, M. Engelcke, and L. Van Der Maaten, “3d semantic segmentation with submanifold sparse convolutional networks,” in *Proceedings of the IEEE Conference on Computer Vision and Pattern Recognition*, 2018, pp. 9224–9232. **4**
- [61] J. Li, S. Bian, A. Zeng, C. Wang, B. Pang, W. Liu, and C. Lu, “Human pose regression with residual log-likelihood estimation,” in *Proceedings of the IEEE/CVF International Conference on Computer Vision*, 2021, pp. 11 025–11 034. **5**
- [62] L. Dinh, J. Sohl-Dickstein, and S. Bengio, “Density estimation using real nvp,” in *Proceedings of the International Conference on Learning Representations*, 2016. **5**
- [63] A. L. Maas, A. Y. Hannun, A. Y. Ng *et al.*, “Rectifier nonlinearities improve neural network acoustic models,” in *Proceedings of the International Conference on Machine Learning*, vol. 30, 2013. **5**
- [64] M. Kristan, J. Matas, A. Leonardis, T. Vojir, R. Pflugfelder, G. Fernandez, G. Nebehay, F. Porikli, and L. Cehovin, “A novel performance evaluation methodology for single-target trackers,” *IEEE Transactions on Pattern Analysis and Machine Intelligence*, p. 2137–2155, 2016. **5**
- [65] Z. Liu, H. Tang, A. Amini, X. Yang, H. Mao, D. L. Rus, and S. Han, “Bevfusion: Multi-task multi-sensor fusion with unified bird’s-eye view representation,” in *Proceedings of the IEEE International Conference on Robotics and Automation*, 2023, pp. 2774–2781. **9**
- [66] X. Bai, Z. Hu, X. Zhu, Q. Huang, Y. Chen, H. Fu, and C.-L. Tai, “Transfusion: Robust lidar-camera fusion for 3d object detection with transformers,” in *Proceedings of the IEEE/CVF Conference on Computer Vision and Pattern Recognition*, 2022, pp. 1090–1099. **9**
- [67] T. Liang, H. Xie, K. Yu, Z. Xia, Z. Lin, Y. Wang, T. Tang, B. Wang, and Z. Tang, “Bevfusion: A simple and robust lidar-camera fusion framework,” *Advances in Neural Information Processing Systems*, vol. 35, pp. 10 421–10 434, 2022. **9**